Detecting Moving Targets in SAR Imagery by Focusing

J. R. FIENUP, Senior Member, IEEE
Veridian Systems

A new method for detecting moving targets in a synthetic aperture radar (SAR) image is presented. It involves segmenting a complex-valued SAR image into patches, focusing each patch separately, and measuring the sharpness increase in the focused patch. The algorithm is sensitive to azimuth velocities and is exquisitely sensitive to radial accelerations of the target, allowing it to detect motion in any direction. It is complementary to conventional Doppler-sensing moving target indicators, which can sense only the radial velocity of rapidly moving targets.

Manuscript received December 9, 1998; revised January 30, 2000 and January 8, 2001; released for publication March 16, 2001.

IEEE Log No. T-AES/37/3/08553.

Refereeing of this contribution was handled by W. D. Blair.

Portions of this paper were presented at the SPIE Conference, April 1995, Orlando, FL.

This work was supported by ERIM Internal Research and Development funds.

Author's address: Veridian Systems, P.O. Box 134008, Ann Arbor, MI 48113-4008, E-mail: (jim.fienup@veridian.com).

I. INTRODUCTION

Detecting the presence of moving targets with an airborne radar is typically performed with a radar that senses the difference in Doppler between the moving target and the fixed background clutter or with a clutter-canceling displaced-phase-center-antenna (DPCA) radar [1, 2], both of which are specifically designed to sense moving targets. These are referred to as moving target indication (MTI) radars. In some instances, when already operating an imaging synthetic aperture radar (SAR) [3, 4], one wishes to detect the presence of the moving target from the available SAR data. We describe a new and powerful moving-target-detection approach that requires only a single conventional complex-valued SAR image. It exploits the fact that target motion induces phase errors that cause a smearing of the target, and these phase errors can be detected by an autofocus algorithm. To reduce false alarms it further requires that the focused image patch have sufficiently increased sharpness over the original image. Because it is computationally efficient, we have used the shear averaging autofocus algorithm [5], but we could use other autofocus algorithms [6–8, ch. 6] as well. This new detection approach is complementary to the traditional approaches in that it is sensitive to the azimuth (cross-range) component of velocity rather than the range component of velocity. It is also exquisitely sensitive to accelerations in range. Consequently it will typically detect targets traveling in any direction.

Like the new approach, the moving-target detection approaches of Moreira and Keydel [9] and of Barbarossa and Scaglione [10] also rely on the motion of the target inducing phase errors and azimuthal smearing of the imagery. In the Moreira and Keydel approach, two or more images are formed from shorter apertures. Images of moving targets in them are displaced in azimuth relative to one another. For each range bin, the intensities of the images are cross-correlated to estimate the quadratic phase error, much like what is done in map-drift autofocus [8, ch. 6]. The quadratic phase error provides a basis, by way of a change in the Doppler rate, for estimating the combined effects of azimuth constant velocity and radial acceleration, and for detecting the motion of the target. In the Barbarossa and Scaglione approach, a product high-order ambiguity function (PHAF) is used to estimate phase errors in each range bin to deduce whether a moving target is present in the range bin. The principal version of the new approach can be expected to have superior performance to both these approaches because it demands that the sharpness of the image significantly improve after focusing. This makes it more robust to false alarms from spurious phase-error estimates. Furthermore, the new approach includes the additional step of segmenting

the image into patches, thereby providing a higher ratio of moving target to background energy when the focusing is performed on each patch (allowing lower velocities to be detected).

Section II describes the approach, shows an example with real data, and discusses its computational requirements and the optimum value of the parameters of the algorithm. Section III reviews the effect of target motion on SAR data. Section IV describes limits placed by the fixed background on the performance of the moving-target detection approach. This includes the results of analysis, of computer simulation, and of experience with real data. Section V draws conclusions.

For the sake of simplicity, we analyze only rigid-body translational motions of the moving target, which cause spatially invariant phase errors; we perform the analysis in the slant plane, ignoring the depression angle; and we assume imaging broadside the SAR, with 90° squint and cone angles.

II. MOVING TARGET DETECTION APPROACH

A. Moving-Target Detection Algorithm

Most target motions induce phase errors in the SAR signal history (often called the "phase history"). These phase errors cause a smearing of the image of the moving target in the cross-track, or azimuth direction. The moving-target detection algorithm is based on the fact that the signal history of the scene as a whole does not have any substantial phase errors, but the component of the signal history corresponding to the blurred image of the moving target has phase errors that we can measure. We employ a fast algorithm, called shear averaging [5], for detecting these phase errors and thereby detect the presence of a moving target; we can also use it to perform a focusing of the moving target, which also adds to our ability to detect it, as described later. Other focusing algorithms could be used as well, but shear averaging has the advantages of being very fast, of being able to detect higher order phase errors, and of not requiring a prominent point scatterer on the target.

Fig. 1 shows a diagram indicating the major steps in the detection approach. We start with a complex-valued SAR image of the entire scene. We interrogate individual patches of the complex image to determine whether there is a moving target in each patch. Let each patch be M pixels in azimuth by N pixels in range, and the image of the entire scene be K by L pixels. Section IIE discusses issues affecting the optimal size of the patches. The procedure that follows is repeated for each patch. The complex image patch is Fourier transformed (in azimuth only) to arrive at the range-compressed signal history for that patch. We perform shear averaging to compute a

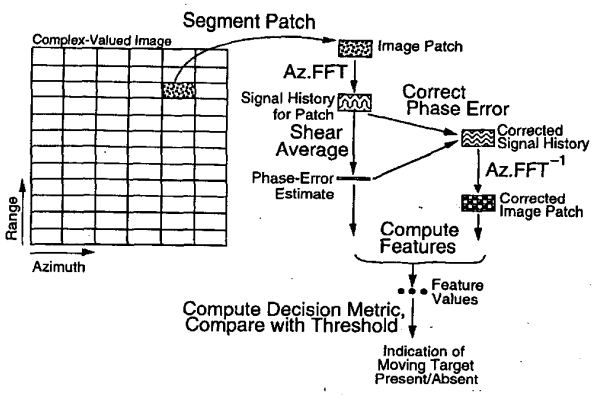

Fig. 1. Approach to detecting moving targets.

phase-error estimate for the patch. We could measure the magnitude of the phase-error estimate and, if it exceeds some threshold, indicate the presence of a moving target. A reasonable measure of the magnitude of the phase-error estimate is its standard deviation

$$f_1 = \phi_{\text{rms}} = \sqrt{M^{-1}\sum_m \phi^2(m) - \left(M^{-1}\sum_m \phi(m)\right)^2}. \tag{1}$$

where $\phi(m)$ is the phase-error estimate for the image patch at the mth azimuth (time) sample, $m = 1,\ldots,M$, after subtracting the linear component of the phase-error estimate (which only translates the image). We have also studied a second feature, the standard deviation of the derivative of the phase-error estimate, but found this to be not as reliable as the standard deviation of the phase-error estimate. A third useful feature is the quadratic component of the phase-error estimate. This is appropriate for many moving targets that induce phase errors that are largely quadratic; however, we have in practice also found that moving targets can induce phase errors that are cubic and higher order, yet have only small quadratic components.

We have also devised a measure of the presence of a moving target that is superior to the magnitude of the phase-error estimate. As indicated in Fig. 1, we correct the data in the patch by subtracting the phase-error estimate from the phase of the signal history for the patch, then inverse Fourier transform to compute the corresponding corrected image for the patch. The ratio of the sharpness of the corrected image patch, to that of the original patch, is a fourth feature that we use to indicate the presence of a moving target. Using the first of the Muller–Buffington image-sharpness metrics [11], we compute the fourth feature as the sharpness ratio

$$f_4 = \frac{\mathbf{S}_1 \text{ (after correction)}}{\mathbf{S}_1 \text{ (before correction)}} = \frac{\sum_{x,y} |g_{\text{cor}}(x,y)|^4}{\sum_{x,y} |g(x,y)|^4}. \tag{2}$$

where $g(x,y)$ is the complex image in the patch before the phase-error correction is applied and $g_{\text{cor}}(x,y)$ is the complex image after the phase-error correction is applied. This fourth power of the complex fields is the same as the square of the image intensity. It measures the degree of concentration of the energy within the image patch. This ratio has proven to be a stronger indication of a moving target than a measure of the phase-error estimate itself, since it will be much larger than unity only if 1) there is a sizable phase-error estimate, and 2) if that phase-error estimate is indeed the correct one, in the sense that it improves the image sharpness.

Note that one can also use this sharpness statistic as the basis of an autofocus algorithm [12–14], and such autofocus algorithms could be used instead of shear averaging. However, these sharpness-based focusing algorithms are several times more computationally demanding than shear averaging.

We have also experimented with other features indicative of a moving target. An example is the degree of image correlation in the azimuth direction. We may combine these various features by using a likelihood ratio test to determine the presence of a moving target. The image sharpness ratio is the single feature that has the best combination of performance and computation speed of the various features we have investigated. For simplicity, here we analyze only the magnitude of the phase error and the sharpness ratio.

The computational requirements of the detection algorithms are dominated by the 1-D fast Fourier transforms (FFTs) used to transform back and forth between the range-compressed signal history and the image. The computational load is comparable to that of the 2-D FFT required to form the image. This computational requirement is less than that of the approach described in [9] and much less than that of the approach described in [10]. The computations for shear averaging, described in the next subsection, are minimal.

The patch size that is optimum for detecting a moving target is one that is roughly the size of the smeared image of the moving target. Larger than optimal patch sizes include excess background, and smaller patch sizes include only a part of the smeared image of the moving target. Nevertheless, the patch width in range should be eight pixels or greater to avoid excessive false alarms. If a wide variety of target velocities are expected, we run the algorithm twice, once with a shorter patch length in azimuth to better detect the shorter smears, and once with a longer patch length in azimuth to better detect the longer smears.

A second way to improve detection performance is to use overlapping patches. Rather than having a patch-to-patch displacement equal to a patch width (i.e., adjacent patches), we may choose patch displacements equal to half the patch width in each dimension.

B. Shear Averaging Algorithm

In this section, we briefly review the shear averaging algorithm [5].

In this section, let the (range-compressed) signal history of a fixed target (or scene) be $F(x,v)$ where x and v are integer pixel numbers. The coordinate x represents range and v represents azimuth (slow time, or pulse number). (We could equally well have x represent frequency, since shear averaging works the same in both the range-compressed signal history and the fully uncompressed signal history.) The phase errors of most concern are in the azimuth dimension only, and we denote them as $\phi_e(v)$. The aberrated signal history is

$$G(x,v) = F(x,v)\exp[i\phi_e(v)]. \tag{3}$$

The corresponding blurred image would be $g(x,y)$, the inverse azimuth Fourier transform of $G(x,v)$.

The shear averaging method consists of the following. In the first step, the shear averaged quantity $S(v)$ is formed by computing the average over the sheared product:

$$S(v) = \sum_{x=1}^{N} G(x,v)G^*(x,v-a) \tag{4}$$

where N is the number of range bins (or, number of samples in frequency) and a is a fixed number of pulses or azimuth samples. Usually $a = 1$ sample. By a derivation similar to that of the van Cittert–Zernike Theorem in optics, it can be shown that [5]

$$\begin{aligned} S(v) &= |S(v)|\exp[i\theta(v)] \\ &\approx N\langle F(x,v)F^*(x,v-a)\rangle \exp[i\phi_e(v) - i\phi_e(v-a)] \\ &= NI_0\mu(0,a)\exp[i\phi_e(v) - i\phi_e(v-a)] \end{aligned} \tag{5}$$

where $\langle\cdot\rangle$ denotes an ensemble average, I_0 is the average aperture-plane intensity, and μ is a correlation coefficient, which is the Fourier transform of the underlying intensity reflectivity of the target or scene, normalized to unity at the origin. From this expression we see that the phase, $\theta(v)$, of $S(v)$ is approximately equal to the difference in phase error from the $(v-a)$th sample to the vth sample. The constant $\mu(0,a)$ may also have a non-zero phase, but that constant phase term will result only in an inconsequential linear term in the phase-error estimate. Therefore an estimate of the phase error can be computed according to

$$\hat{\phi}_e(0) = 0 \qquad \text{and} \qquad \hat{\phi}_e(v) = \hat{\phi}_e(v-a) + \theta(v) \tag{6}$$

or, equivalently,

$$\hat{\phi}_e(v) = \sum_{m=1}^{v/a} \theta(ma). \tag{7}$$

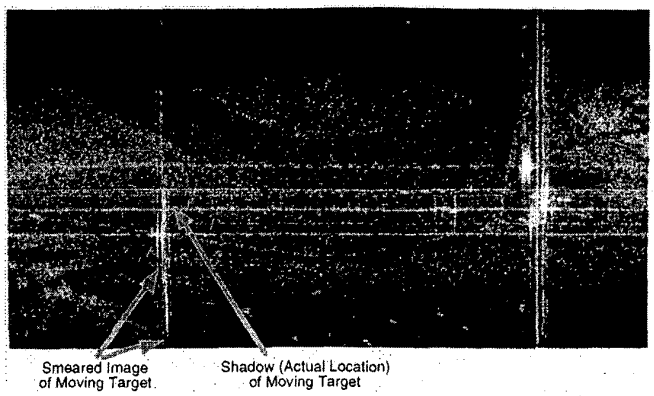

Fig. 2. Magnitude of ADTS image. Smeared image of moving schoolbus seen in lower left portion of image. Range is horizontal and azimuth is vertical.

This phase-error estimate is subtracted from the phase of $G(x,v)$ to arrive at a phase-error-corrected version of the signal history $G_{\text{cor}}(x,v)$. Note that subtraction of a phase can be accomplished by a complex phasor multiplication. The summation of the phase differences in (7) can likewise be done by the multiplication of phasors. The corresponding corrected image would be $g_{\text{cor}}(x,y)$, the inverse Fourier transform of $G_{\text{cor}}(x,v)$.

The result in (5) above depends on approximating the finite sum in (4) by an ensemble average, and the accuracy of this approximation depends on the number N of range bins (or frequency bins) over which we average (for the case of a complicated object or clutter scene). The accuracy of the phase-error estimate also depends on the number M of azimuth bins over which we sum. The result is that the standard deviation of the phase error at the Mth sample is approximately

$$\sigma_M = \frac{1}{|\mu(0,a)|}\sqrt{\frac{M}{2N}}. \tag{8}$$

Ordinarily we choose the shear distance $a = 1$ sample in azimuth (pulse number) in the signal history. The value of $|\mu(0,1)|$ depends on the oversampling of the signal history and the content of the image. For a twice-Nyquist sampled signal history (oversampling is necessary in SARs anyway to avoid aliasing) of a uniformly reflecting scene, $|\mu(0,1)| \approx 0.7$. The weighting of the image by the antenna illumination function in the spatial domain will ordinarily provide the needed oversampling in the signal history domain. However, for an extracted image patch over which the weighting of antenna illumination is not evident, the situation is different. For a patch of uniformly reflecting (clutter) area we will have $|\mu(0,1)| \approx 0$, and $|\mu(0,1)|$ increases as the scene becomes more highly structured, becoming unity when the scene consists of a single delta function. For the case of an image patch containing the smeared image of a moving target, ordinarily the focused image of the moving target (which is what counts for the value of $|\mu(0,1)|$) would be a fraction of the patch width, making its signal history highly oversampled, making $|\mu(0,1)|$ be near unity, even if the width of the smeared image is equal to the patch width.

Therefore for typical signal histories having $M = N$ and for shear a such that $|\mu(0,a)| \approx 0.7$ (requiring a two-fold oversampling in the v direction), the expected residual phase error will be about 1 rad ($\lambda/6$) peak-to-valley. However, the phase-error estimate for the image patch will be for the sum of the moving target image and the background image. Since the background presumably has no phase error associated with it, that sum is expected to have a phase-error estimate that is less than the true phase error for the moving target alone. For these reasons, the phase-error estimate provided by shear averaging is not necessarily expected to be faithful enough to completely correct the smeared image of the moving target (although in many cases it will be faithful). Nevertheless, the phase-error estimate is highly likely to be adequate for moving-target detection since it must merely exceed some threshold, or increase the sharpness of the image sufficiently, to distinguish a patch containing a moving target from a patch containing no moving target. More sophisticated phase-error correction algorithms can be used to yield better detection performance, but at the cost of greater computational complexity.

C. Detection Example

Fig. 2 shows an image to which we applied the detection algorithm. The data was collected by MIT Lincoln Laboratory's ADTS 33.56 GHz SAR [15, 16], which has 1 ft resolution in range (see the Table I in the next section). The image, of size 2048 pixels in range by 708 pixels in azimuth, contains a smeared image of a schoolbus moving in a circle at a speed of about 20 mi/h. A corner reflector had been mounted on the top of the vehicle to enhance its return. We formed the image by simply azimuth Fourier transforming 708 range-compressed pulses, equivalent

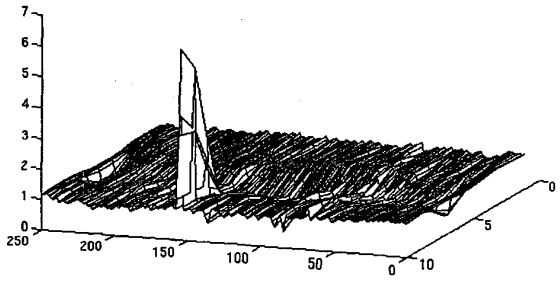

Fig. 3. Detection result. Image patches having increased sharpness of about 2.0, or greater, are likely to contain moving targets.

to 0.472 s of data. Since we did not perform polar interpolation, the images we produced are slightly smeared away from the center of the scene. This smearing was small because 1) at 33.56 GHz a smaller angular aperture is needed than at lower frequencies, 2) we used less than half the normal azimuth aperture needed to get 1 ft resolution, and thereby avoided false alarms due to lack of polar interpolation in this case. Nevertheless, the image is adequate for demonstrating our detection algorithm. We used a patch size of 16 pixels in range by 128 pixels in azimuth, and used four overlapping grids of patches. Fig. 3 shows the sharpness ratio for the patches in a perspective plot. The maximum value, 6.2, of the sharpness ratio f_4 exceeds the typical threshold of 2.0 by over a factor of three, giving a strong indication of a moving target. The algorithm indicates the presence of a moving target only in the area in which the smeared image of the schoolbus appears. Despite the presence of other bright (nonmoving) targets in the image, there are no false alarms.

Fig. 4 shows the focusing results on two different image chips. Fig. 4(a) shows the chip that contains most of the smear from the moving target (the square root is shown to stretch the contrast). It clips off the top end of the smear. Fig. 4(b) shows the corresponding image focused by shear averaging. It occupies an area several times smaller than that of the given smeared image, making the sharpness of the focused chip increase by a factor of greater than six times that of the original chip. Fig. 4(c) and (d) show the same things for a chip containing only clutter background, located 40 pixels to the left of the chip containing the target. Although the focusing algorithm rearranged the energy somewhat, it did not cause its sharpness to increase, the sharpness ratio being $f_4 = 0.95$.

Fig. 5 shows the phase error estimates for the two cases, the upper curve for the chip having the moving target and the lower curve for the chip containing background only. For both cases the linear trends were removed. The phase-error estimate for the moving target is, as is often the case, a large and

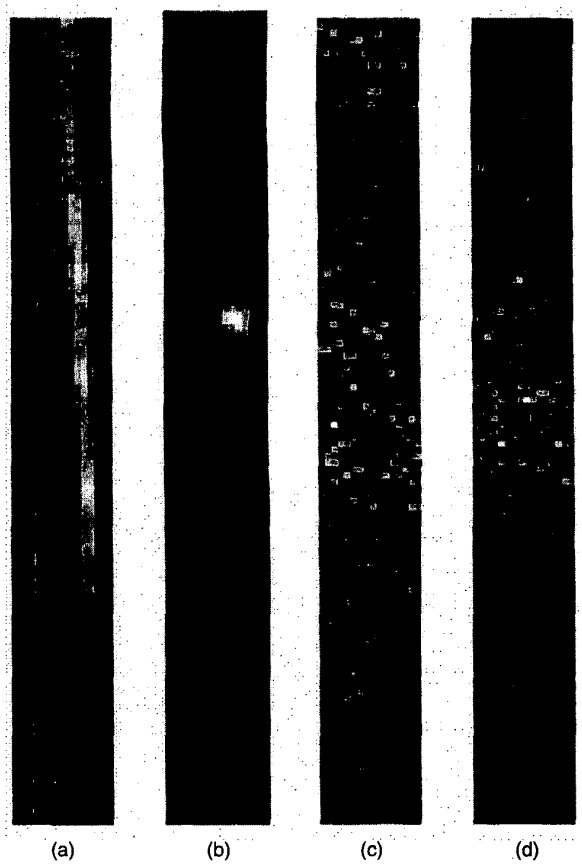

Fig. 4. Focused chips. (a) Image patch including smeared image of moving target. (b) Focused image of chip (a). (c) Image patch of clutter background only. (d) Focused image of chip (c).

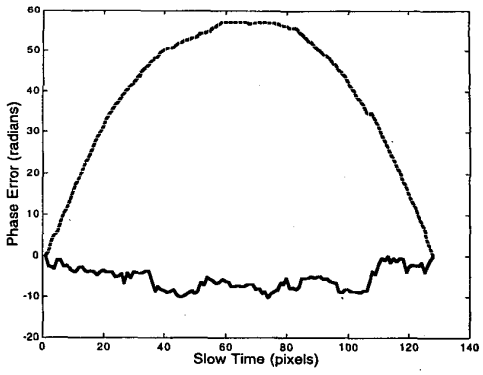

Fig. 5. Phase error estimates. Upper (dashed) curve: phase-error estimate for chip including target. Lower (solid) curve: phase-error estimate for chip including clutter background only.

relatively smooth function, and it is predominantly quadratic. The phase-error estimate for the fixed clutter background is more random, and is smaller. As discussed above, shear averaging has a residual error that depends on the degree of oversampling of the signal history in the slow-time direction. Since the clutter background fills the image chip in azimuth,

TABLE I
System and Target Parameters

Symbol	Description	Example Value
v_p	platform velocity	100 m/s
T	aperture time	1.30 s
t	slow time	variable
R_0	range to scene center	7250 m
$\Delta\theta_a$	aperture angle = v_pT/R_0	0.0179 rad. (1.024°)
x	image slant-range coordinate	variable
y	image azimuth coordinate	variable
(x_0,y_0)	coordinates of target point	various
v_r	target range velocity	4.47 m/s (10 mph)
v_a	target azimuth velocity	4.47 m/s (10 mph)
a_r	target range acceleration	0.172 m/s^2 (0.5 mph/T)
f_0	center frequency	33.56 GHz
f	instantaneous frequency	variable
f'	relative frequency $(f-f_0)$	variable
Δf	bandwidth $(f_{max}-f_{min})$	600 MHz
$\Delta f/f_0$	fractional bandwidth	0.0179 = 1/55.9
λ_0	center wavelength	8.94 mm
c	speed of light	3×10^8 m/s
ρ_r	(unweighted) range resolution	0.25 m
ρ_a	(unweighted) azimuth resolution	0.25 m
k_r	range weighting factor	1.2
k_a	azimuth weighting factor	1.2
d_r	distance target moves in range = v_rT	5.8 m
d_a	distance target moves in azimuth = v_aT	5.8 m

the signal history is close to being critically sampled, making $|\mu(0,a)|$ relatively small and making the phase error, which takes the form of the random walk shown in the lower curve of Fig. 5, moderately large (about 10 rad peak-to-valley in this example). This erroneous phase does not cause the image chip to become better focused, and hence decreases rather than increases the sharpness. In contrast to this, the focused image of the moving target, as seen in Fig. 4(b), occupies a small portion of the image chip in azimuth, making its signal history well over-sampled, making $|\mu(0,a)|$ near unity, and making the error in the phase-error estimate (the upper curve in Fig. 5) small.

III. ANALYSIS OF SAR PHASE ERRORS FROM TRANSLATIONAL MOTIONS

In this section, we review the type of phase errors and image translation induced in a spotlight SAR [3, 4, 8] signal history by target translational motion. Consider a SAR with parameters given in Table I. The values given are for example calculations and are consistent with MIT Lincoln Laboratory's ADTS system, and a target moving with 10 mi/h components of velocity in both the range and azimuth directions. For simplicity we consider the case of imaging broadside to the SAR platform and ignore the depression angle.

The resolutions in azimuth and in slant-range for an unweighted aperture are given by

$$\rho_a = \frac{\lambda_0 R_0}{2v_pT} = \frac{\lambda_0}{2\Delta\theta_a} \tag{9}$$

and

$$\rho_r = \frac{c}{2\Delta f} = \lambda_0\frac{f_0}{2\Delta f}. \tag{10}$$

The actual resolutions are $k_a\rho_a$ and $k_r\rho_r$, respectively, where k_a and k_r are factors that account for the coarsening of resolution owing to such things as weighting functions for sidelobe control.

For simplicity, consider the case of a point target moving with constant component of velocity in azimuth, and a velocity and an acceleration in slant-range. For simplicity suppose that the target motion is in the slant plane. The phase error for a complicated target experiencing rigid-body translational motion will be the same as that computed here for a point target. The target has instantaneous position

$$(x,y) = (x_0 + v_rt + \tfrac{1}{2}a_rt^2, y_0 + v_at), \quad -T/2 \le t \le T/2 \tag{11}$$

making the instantaneous range velocity $v_r + a_rt$. In a spotlight-SAR signal history the phase is compensated for a fixed point at the scene center. The phase of the signal history is proportional to r, the distance from a point on the flight path to the target point, minus the distance from the point on the flight path to the scene center:

$$\phi(f',t) = \frac{4\pi}{\lambda}\left(r - \sqrt{R_0^2 + (v_pt)^2}\right) \tag{12}$$

where

$$r = \sqrt{(R_0 + x_0 + v_rt + \tfrac{1}{2}a_rt^2)^2 + (y_0 + v_at - v_pt)^2} \tag{13}$$

and

$$\frac{1}{\lambda} = \frac{f}{c} = \frac{(f_0+f')}{c} = \frac{1}{\lambda_0}\left(1 + \frac{f'}{f_0}\right). \tag{14}$$

Performing a Taylor series expansion, we have

$$\phi(f',t) = \frac{4\pi}{\lambda_0}\left[x_0 + x_0\frac{f'}{f_0} - y_0\frac{v_pt}{R_0} + v_rt + \frac{1}{2}a_rt^2 - \frac{v_a}{v_p}\frac{(v_pt)^2}{R_0} - \frac{v_a}{v_p}\frac{f'}{f_0}\frac{(v_pt)^2}{R_0} + \cdots\right]. \tag{15}$$

The given terms are described in Table II. The last column of the table gives values for the case in Table I of a moving target with velocity v_r or v_a = 4.47 m/s (10 mi/h) or a_r = 0.0172 m/s^2 (a_rT = 0.5 mi/h). Note, for comparison, that the distance traveled by a target with velocity 4.47 m/s in time T = 1.3 s is 5.8 m.

TABLE II
Phase Terms for a Moving Point

Phase term $\phi(f',t)$	Description	Results in	Example Value
$\frac{4\pi}{\lambda_0}x_0$	constant phase	phase constant (unimportant here)	
$\frac{4\pi}{\lambda_0}x_0\frac{f'}{f_0}$	frequency linear phase	range position x_0	various
$\frac{4\pi}{\lambda_0}y_0\frac{v_p t}{R_0}$	azimuth linear Phase	azimuth position y_0	various
$\frac{4\pi}{\lambda_0}v_r t$	Range-velocity-induced azimuth shift	Azimuth translation by $\frac{4\pi}{\lambda_0}\frac{v_r T\rho_a}{2\pi} = \frac{v_r R_0}{v_p} = \frac{R_0}{v_p T}d_r = \frac{d_r}{\Delta\theta_a}$	324 m
$\frac{4\pi}{\lambda_0}\frac{1}{2}a_r t^2$	Range-acceleration-induced azimuth quadratic phase	Azimuth smear of 8(# waves quad. phase) ρ_a $= 2\frac{a_r T^2\rho_a}{\lambda_0} = \frac{a_r T R_0}{v_p}$	16.2 m
$\frac{4\pi}{\lambda_0}\frac{v_a v_p t^2}{R_0}$	Azimuth-velocity-induced azimuth quadratic phase	Azimuth smear of 8(# waves quad. phase) ρ_a $= 2v_a T = 2d_a$	11.6 m
$\frac{4\pi}{\lambda_0}\frac{f'}{f_0}\frac{v_a v_p t^2}{R_0}$	Azimuth-velocity-induced range walk	Range walk of smear = (azimuth smear) $\frac{\Delta\theta_a}{4}$	0.0725 m

Note: Example values are for system and motion parameters in Table I.

From Table II, we see that the phase error due to the azimuth-velocity-induced range-walk term is a small fraction of the azimuth smear due to the azimuth-velocity-induced quadratic phase error. Consequently, for estimating the phase error to detect the presence of a moving target, we can usually ignore this phase term. However, for accurately correcting the phase error, this term can be significant for fast-moving targets. This term causes a small but noticeable curvature to the smeared image when the smearing is very large. Range acceleration induces a similar range-walk term. Polar interpolation [3, 8] affects none of the purely azimuthal terms in Table II, and so we ignore its effects here.

If polar interpolation is not performed, then there are additional quadratic phase terms, which increase linearly with the distance from the scene center, smearing the fixed background. So for effective detection in spotlight SAR imagery, polar interpolation should be performed or the detection should be limited to the central portion of the image.

The three major terms of concern are 1) the image translation in azimuth due to a constant component of velocity in range, 2) the azimuth smearing due to a constant component of acceleration in range, and 3) the azimuth smearing due to a constant component of velocity in azimuth. The first causes the image of the moving target to fall on top of an area of the scene that is distant from the area where the target is physically located; and the latter two, resulting from quadratic phase errors, cause a smearing in azimuth that results in a reduction in both the brightness and the intelligibility of the image of the moving target.

In general, a quadratic phase error

$$\phi(t) = \frac{2\pi A t^2}{(T/2)^2} = \frac{8\pi A t^2}{T^2} \tag{16}$$

defined over an aperture $-T/2 \le t \le T/2$ has center-to-edge amplitude A cycles ($2\pi A$ rad) and has standard deviation

$$\sigma_\phi = 2\pi A\frac{2}{3\sqrt{5}}. \tag{17}$$

Since the derivative of $\phi(t)$ is $4\pi At/(T/2)^2$, its maximum (minimum) derivative is $(-)8\pi A/T$. A linear phase having this slope over the entire aperture T would have an excursion of $(-)8\pi A$ rad. Since a Fourier-domain linear phase of 2π rad shifts an image by ρ_a, portions of the image are smeared over the interval $-4A\rho_a$ to $4A\rho_a$, for an image smear of length

$$\text{(azimuth smear)} = 8A\rho_a. \tag{18}$$

This relationship is true when the azimuth smearing is much greater than one resolution element. When the smearing is small, this approximation overstates the smearing, and a better approximation is (azimuth smear) $= \rho_a\sqrt{k_a^2 + (8A)^2}$.

If aperture weighting is present, then the deleterious effect of the phase error tends to be reduced since the weighting function reduces the signal history most where the phase error tends to be the greatest, near the edge of the aperture. However, the effect of aperture weighting is *not* to reduce the length of the smear. For quadratic and higher even-order phase errors, the effect is to reduce the intensity of the smear near the ends of the smear. Hence the 3 dB width of the smear decreases without the length of the smear decreasing.

Since the azimuth-velocity-induced azimuth quadratic phase error has

$$A = \frac{v_a T}{4} \frac{2v_p T}{\lambda_0 R_0} = \frac{d_a}{4\rho_a} \tag{19}$$

where $d_a = v_a T$ is the distance the target moves in azimuth during the aperture time, we find that the standard deviation of the phase error for an unweighted aperture is

$$\sigma_\phi = \frac{\pi}{3\sqrt{5}} \frac{d_a}{\rho_a} \tag{20}$$

and the azimuth smear length is

$$\text{(azimuth smear)} = 2d_a. \tag{21}$$

The number of unweighted resolution elements of the azimuth smear is

$$M_a = \frac{\text{(azimuth smear)}}{\rho_a} = \frac{2(v_a T)}{\rho_a} = \frac{2d_a}{\rho_a}. \tag{22}$$

For the example parameters in Table I, the azimuth smear is 11.6 m = $46.5\rho_a$, equivalent to 5.8 cycles of quadratic phase error. As we see later, we expect to detect bright moving targets that smear by $2\rho_a$, or $M_a = 2$; therefore, we expect to be able to detect an azimuth velocity of 1/23 of the example, or 0.19 m/s (0.43 mi/h), for a favorable case.

Since the range-acceleration-induced quadratic phase error has

$$A = \frac{a_r T^2}{4\lambda_0} \tag{23}$$

we find that the azimuth smear length is

$$\text{(azimuth smear)} = 8A\rho_a = \frac{2a_r T^2 \rho_a}{\lambda_0} = d_r \frac{4\rho_a}{\lambda_0}$$

$$= d_r \frac{2R_0}{v_p T} = \frac{2d_r}{\Delta\theta_a}. \tag{24}$$

In this expression, $d_r = (1/2)a_r T^2$, which is the distance the target would travel in time T had it started from rest and accelerated at the rate of a_r. Another useful way to express this is to note that the range velocity changes by $a_r T$ during the aperture time. The azimuth smear is $2(a_r T)\rho_a T/\lambda_0$, which, expressed in the number of unweighted resolution elements, is

$$M_r = \frac{\text{(azimuth smear)}}{\rho_a} = \frac{2(a_r T)T}{\lambda_0}. \tag{25}$$

Since for the ADTS SAR $\rho_a/\lambda_0 \approx 28$, the azimuth smear is about $56(a_r T)T$, that is, 56 times the distance given by the change in radial velocity $(a_r T)$, times the aperture time T. From the example values in Table I, an $(a_r T)$ change of range velocity of 0.5 mi/h results in an azimuth smearing of 16.2 m. Hence very small accelerations in range can result in considerable azimuth smearing; consequently small accelerations in range allow us to detect the moving target.

If the target's acceleration is time varying, then higher order phase terms are introduced. In particular, if the range coordinate of the target is described by an nth-order polynomial in time, then the motion introduces an nth-order polynomial azimuth phase error; and if the azimuth coordinate is described by an nth-order polynomial in time, then the motion introduces an $(n+1)$-order polynomial azimuth phase error. As long as the focusing algorithm can correct higher order phase errors (as shear averaging can), these higher order motions contribute to the ability to detect the moving target as well.

IV. DETECTION PERFORMANCE IN THE PRESENCE OF FIXED BACKGROUND

We determined the detection performance of the algorithm in three ways: 1) by theoretical calculations, 2) by computer simulations, and 3) by testing on real data. Unfortunately, because of a lack of a sufficient number of images of ground-truthed moving targets, the results we have with real data are not statistically meaningful, but do serve as examples.

A. Theoretical Performance Prediction

We performed the analysis for two detection features: f_1, the rms phase-error estimate, and f_4, the sharpness ratio. We found the latter to be the more effective means of detecting moving targets and consider it our primary statistic, but for the sake of completeness we report below on the results for both features.

We predicted the performance theoretically with the following steps. First, we predict the phase errors induced by a given target motion (azimuth velocity or radial acceleration). Next we take into account the fact that a given patch of the image contains both the smeared image of the moving target and the background, which is well focused and has no phase errors. The consequence of the background is that the phase error estimated for the patch will be less than the phase error appropriate for the target. The phase error is underestimated more for smaller target-to-background ratios. The phase error is also underestimated more for more highly structured backgrounds than for uniform clutter backgrounds. The structure of the background is quantified by $|\mu_g|$, the correlation coefficient for the background. We

assume, for simplicity, that the moving target has only a single bright scatterer in each range bin. Then if there were no background and we were to perfectly focus the moving target, its sharpness would increase by a factor of M_a, the number of resolution elements by which the image of the target was smeared. The minimum detectable velocity derived here should be taken to be a lower bound, since targets having multiple closely spaced scatterers within a given range bin will require higher velocities for detection. The total sharpness of the patch is also affected by the sharpness and brightness of the background. After focusing the patch according to the underestimated phase error, the target is partially focused, increasing its sharpness, and the background is defocused, decreasing its sharpness.

We analyzed the theory for the simplest possible case: that of the moving target consisting of a single bright point (a delta function) having a constant velocity in azimuth, resulting in a quadratic phase error. We analyze the cases of the background consisting of either zero-mean Gaussian-distributed complex-valued clutter or a single bright corner reflector. For simplicity we assume an unweighted aperture with no zero-padding.

1) *Shear Averaging Phase-Error Estimate*:

a) *Phase-error estimate for the target only*: First, we assume that the target point source is centered in the image patch, making its reflectivity $f_t(x,y) = b\delta(x,y)$, where the origin of the coordinates of the patch is in the center of the patch and $\delta(x,y)$ is the Kronecker delta function in two dimensions. The target's azimuth Fourier transform is $F_t(x,v) = bM^{-1/2}\delta(x)$, and with motion the signal history is

$$G_t(x,v) = bM^{-1/2}\delta(x)\exp[i\phi_t(v)] \tag{26}$$

where b is a complex constant. M is the number of image pixels (resolution elements) in azimuth and N the number in range in the patch. The factor of $M^{-1/2}$ arises if we employ a version of the discrete Fourier transform which is unitary, that is, energy-preserving. The sheared sum for the target alone is

$$\begin{aligned} S_t(v) &= |S_t(v)|\exp[i\theta_t(v)] \\ &= |b|^2M^{-1}\exp[i\phi_t(v) - i\phi_t(v-a)] \end{aligned} \tag{27}$$

making the phase of the sheared sum

$$\theta_t(v) = \phi_t(v) - \phi_t(v-a) \tag{28}$$

which makes the phase-error estimate

$$\hat{\phi}_e(v) = \sum_{m=1}^{v/a}\theta_t(ma) = \phi_t(v) \tag{29}$$

that is, the phase-error estimate from shear averaging is exactly correct (up to an unimportant additive constant) when only a delta-function target is present.

If there is no moving target and only a background $F_g(x,v)$, then the sheared sum is

$$\begin{aligned} S_g(v) &= |S_g(v)|\exp[i\theta_g(v)] = \sum_x F_g(x,v)F_g^*(x,v-a) \\ &\approx NI_g|\mu_g(a)|\exp[i\theta_g(v)] \end{aligned} \tag{30}$$

where I_g is the average energy per pixel in the background. More generally the magnitude of this expression will vary with v as well (which we have ignored); but it is the phase variation $\theta_g(v)$ that will have the largest impact. When the background alone is present, the phase of the sheared sum is

$$\theta(v) = \theta_g(v) \tag{31}$$

and the phase-error estimate from shear averaging is given by

$$\hat{\phi}_e(v) = \phi_g(v) = \sum_{m=1}^{v/a}\theta_g(ma). \tag{32}$$

The phase-error estimate for only the background depends on the correlation properties of the underlying reflectivity of the background. If the background is highly structured, then the shear averaging algorithm will tend to produce a phase-error estimate that is near to zero. At the opposite extreme, for which the background is completely unstructured, i.e., it is perfectly uniform clutter, the phase-error estimate can be quite large. Since perfectly uniform clutter does sometimes occur in nature (a grassy field, for example), this case is of practical interest. Note that perfectly uniform clutter may cause a large phase-error estimate, making it a potential false alarm for f_1, the rms phase error, but it will not cause a false alarm for f_4, the sharpness ratio.

For Nyquist-sampled data from a patch of perfectly uniform clutter, $|\mu_g(a=1)| = 0$, and the phase differences θ_g predicted by shear averaging are random numbers uniformly distributed on $[-\pi,\pi)$ rad. The phase-error estimate is given by a sum of M such random numbers, where M is the number of sample in azimuth in the patch. This defines a random walk problem. However, the linear component of the phase only shifts the image and does not contribute to the smearing of the image. Consequently, we should remove the linear component of the phase before calculating its magnitude. After doing this, we can show that the expected value of the standard deviation of the phase-error estimate (actually, the square root of the expected variance), averaged over the M samples, is

$$\sigma_1 = \frac{\pi}{6}\sqrt{M}. \tag{33}$$

For example, if $M = 128$ azimuth samples, the expected rms phase error is 5.9 rad, which is substantial. This compares with the standard deviation of the phase error induced by a moving target having

an azimuth velocity v_a, we saw earlier is given by $\sigma_\phi = (\pi/3\sqrt{5})d_a/\rho_a$. Recall that the azimuth smearing for this velocity is $M_a = 2d_a/\rho_a$ unweighted resolution elements. The optimum patch size (in unweighted resolution elements) M, in azimuth, is one large enough to just enclose the smeared image of the moving target. This would be M_a for a smear large compared with the target size. Inserting this expression into the equation above for the expected rms phase error due to pure uniform clutter alone, for $M = M_a$ (azimuth unweighted resolution elements), we get

$$\sigma_1 = \frac{\pi}{6}\sqrt{\frac{2d_a}{\rho_a}}. \tag{34}$$

Taking the ratio of the standard deviation of the phase error due to a moving target, with azimuth velocity v_a traveling a distance d_a in time T, and that due to pure uniform clutter over a patch size equal to the length of the smear due to the target motion, we have the ratio

$$\frac{\sigma_\phi(\text{target only})}{\sigma_1(\text{clutter only})} = \sqrt{\frac{2}{5}\frac{d_a}{\rho_a}}. \tag{35}$$

This would indicate that if the target moves by several resolution elements in azimuth during the aperture time, then it will induce a phase error that is considerably greater than the expected phase-error estimate from worst case clutter alone.

b) *Phase estimate for target plus background*: Now consider the case of combined signals—target plus background—given by

$$G(x,v) = G_t(x,v) + F_g(x,v) \tag{36}$$

where $G_t(x,v) = bM^{-1/2}\delta(x)\exp[i\phi_t(v)]$ for our simple point target. We can show that the sheared sum of this combined target-plus-background case is given approximately by

$$\begin{aligned} S(v) &= |S(v)|\exp[i\theta(v)] \\ &\approx |b|^2 M^{-1}\exp[i\theta_t(v)] + NI_g|\mu_g(a)|\exp[i\theta_g(v)] \end{aligned} \tag{37}$$

and its phase is given approximately by

$$\theta(v) \approx k_t\theta_t(v) + (1-k_t)\theta_g(v) \tag{38}$$

where

$$k_t = \frac{|b|^2}{|b|^2 + MNI_g|\mu_g(a)|} \tag{39}$$

is the $|\mu|$-weighted ratio of the energy of the moving target to the total energy of the patch, and $(1-k_t)$ is the $|\mu|$-weighted ratio of the energy of the background to the total energy of the patch. Note that $|\mu| = 1$ for the point target. From this we see that when the target energy dominates over the background energy, we detect most of the phase error due to the moving target. For a clutter background that is very uniform, $|\mu_g(a)|$ will be small and the moving target's phase error will be underestimated less.

2) *Performance Prediction for Sharpness Ratio*: The sharpness ratio f_4 given by (2), is our primary indicator of moving targets. Consider the specific case of a target traveling with constant velocity v_a in azimuth. This motion results in a simple quadratic phase error, and the resulting image is smeared in azimuth by the number of unweighted resolution elements $M_a = 2d_a/\rho_a$, for $M_a \gg 1$. For a quadratic phase error, in the smeared image the energy tends to be spread uniformly over the distance of the smear, for an unweighted aperture. That is, instead of the intensity $|b|^2$ of the point target being concentrated in a single pixel, it is spread uniformly over M_a unweighted resolution elements, each of which would have intensity $|b|^2/M_a$ (owing to conservation of energy). If the energy of the target far exceeded that of the background in the patch, then the shear averaging algorithm would successfully correct the phase error, returning all the energy to a single resolution element. Then the numerator of the sharpness ratio would be $|b|^4 \times$ (one resolution element) $= |b|^4$, and the denominator would be $(|b|^2/M_a)^2 \times M_a = |b|^4/M_a$, making the ratio $f_4 = M_a$. Assuming that we need $f_4 = 2$ for a solid indication of a moving target (which we have experienced is a conservative threshold in order to eliminate most all false alarms in clutter backgrounds), then for a reliable detection we need

$$M_a \geq 2 \tag{40}$$

in the ideal case. This condition is equivalent to $d_a \geq \rho_a$, which is equivalent to a minimum detectable azimuth velocity of

$$v_a \geq \frac{\rho_a}{T} = \frac{\lambda_0 R_0}{2v_p T^2}. \tag{41}$$

For the example parameters in Table I, $M_a = 46$ resolution elements, which is 23 times the minimum required for detection. The minimum detectable azimuth velocity for that example would be $v_a =$ 0.19 m/s. The minimum detectable radial acceleration would be $a_r = \lambda_0/T^2$, and the minimum detectable change in radial velocity would be

$$(a_r T) \geq \frac{\lambda_0}{T} \tag{42}$$

which is a radial velocity change of only 6.9 mm/s (0.015 mi/h) for the parameters in Table I. Hence we see that, even though it is insensitive to constant radial velocities, the approach can be exquisitely sensitive to changes in radial velocity. Since small radial accelerations are present in most real moving targets, this algorithm should be able to detect targets moving in any direction.

Note that if we hold all other parameters (λ_0, R_0, v_p) constant, the minimum detectable azimuth

velocity and radial acceleration both increase as $1/T^2$, and hence as ρ_a^2, the square of the azimuth resolution.

If we employ aperture weighting, the minimum detectable azimuth velocity should increase because 1) the sharpness of the original smeared image will be greater than for an unweighted aperture, since aperture weighting causes the center of the smear to be brighter than the edges of the smear, and 2) the sharpness of the focused image will be less than for an unweighted aperture, since aperture weighting causes the mainlobe of the diffraction-limited impulse response to be wider than for an unweighted aperture. Hence, for detecting moving targets we expect to obtain better performance if we employ an unweighted aperture.

Since the estimate above depends on the background energy being negligible, the target being a single bright point source (such as a corner reflector), the aperture being unweighted, and the patch length being optimum, the minimum detectable azimuth velocity (and minimum detectable change in radial velocity) will often be greater than this.

Next we consider a more complete theory, which includes the effect of the background on the sharpness ratio. We consider two cases, which differ significantly from one another. The first is a relatively benign case, for which the background is uniform clutter. As we focus the moving target, making its sharpness increase, the defocusing of the clutter does not change its sharpness much; hence, the net sharpness increases. For this reason, uniform clutter is relatively benign. The second is the most difficult case, for which the background consists of a single bright pixel in the same image patch. As the moving target is focused and the background point becomes defocused, the sharpness of the background point will decrease substantially; hence the net sharpness increases only if the moving target is considerably brighter than the background point.

For both cases, suppose that we choose a patch azimuth length $M \geq M_a$, which is necessary to avoid truncating the smeared image of the moving target, and we position the patch so that the smeared image of the target falls entirely within it. The intensity of the focused target point would $|b|^2$, making the intensity of the smeared image of the target point, per unweighted resolution element, be $|b|^2/M_a$ in its non-zero range bin over the extent of its smear (it is zero in the other range bins). The presence of the background will usually cause us to underestimate the phase error due to the moving target. Suppose that our phase-error estimate is a constant α times the true phase error associated with the moving target, with $0 \leq \alpha \leq 1$. After correction, the target will focus to a smear of approximate length $M_a + \alpha(1 - M_a)$; that is, it will have length M_a if no focusing is done ($\alpha = 0$) and length 1 pixel if the focusing is perfect ($\alpha = 1$). Hence the sharpness contribution due to the focused moving target is

$$\mathbf{S}_{1t}(\alpha) = \left(\frac{|b|^2}{[M_a + \alpha(1 - M_a)]}\right)^2 \times [M_a + \alpha(1 - M_a)] = \frac{|b|^4}{[M_a + \alpha(1M_a)]}. \tag{43}$$

If α is large enough that the smear length of the corrected image is just a couple of pixels or less, then the expression $M_a + \alpha(1 - M_a)$ will overestimate the smear length, which will tend to underestimate the sharpness of the focused point. Consequently, this approximation causes us to underestimate the increase in sharpness after focusing, and is therefore conservative.

a) *Sharpness ratio—clutter background*: First consider the case of a clutter background that is relatively uniform. If the average energy per unweighted resolution element of the clutter in the patch is I_g, then the sharpness contribution due to the focused, relatively uniform clutter is

$$\mathbf{S}_{1g} = 2I_g^2 MN \tag{44}$$

where N is the range width of the patch and the factor of two arises from the negative exponential statistics of the intensity of the clutter. Suppose that the clutter is sufficiently uniform that changing its focus does not affect its sharpness much. However, at the same time we assume that $|\mu_g|$ is large enough that the background does influence the phase-error estimate. If we ignore the cross term between the target and the clutter, the total sharpness is

$$\mathbf{S}_1(\alpha) = \mathbf{S}_{1t}(\alpha) + \mathbf{S}_{1g} = \frac{|b|^4}{[M_a + \alpha(1M_a)]} + 2I_g^2 MN. \tag{45}$$

The sharpness for $\alpha = 0$ (for no focusing, giving the sharpness of the original patch) is

$$\mathbf{S}_1(0) = |b|^4/M_a + 2I_g^2 MN \tag{46}$$

and so the sharpness ratio is

$$f_4 = \frac{\mathbf{S}_1(\alpha}{\mathbf{S}_1(0)} = \frac{\dfrac{|b|^4}{[M_a + \alpha(1 - M_a)]} + 2I_g^2 MN}{|b|^4/M_a + 2I_g^2 MN}. \tag{47}$$

Recalling that the phase-error difference estimate will be approximately $\theta \approx k_t\theta_t + (1 - k_t)\theta_g$, and letting $\theta_g \approx 0$, we have $\theta \approx k_t\theta_t$. Noting that $\alpha = \theta/\theta_t$, we have

$$\alpha \approx k_t = \frac{|b|^2}{|b|^2 + MNI_g|\mu_g|}. \tag{48}$$

Inserting this into the equation above and rearranging terms yields

$$f_4 = \frac{\dfrac{K_{ta}^2 M_a N(K_{ta} + M|\mu_g|)}{(K_{ta} + M_a M|\mu_g|)} + 2M_a M}{K_{ta}^2 N + 2M_a M} \tag{49}$$

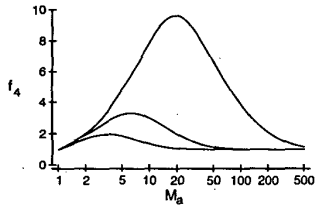

Fig. 6. Predicted sharpness ratio as function of smear length for uniform clutter background. For $N = 16$, $M = M_a$, $|\mu_g| = 0.3$, and for target/background ratio per azimuth bin of $K_{ta} = 100$ (upper curve), 10 (middle curve), and 3 (lower curve).

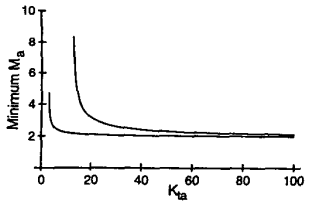

Fig. 7. Minimum smear length versus target-to-background ratio, for clutter background. For $|\mu_g| = 0.1$, $N = 16$, to achieve $f_{4t} = 2$. Patch length: Upper curve, $M = 64$; lower curve, $M = 8$.

where

$$K_{ta} = \frac{|b|^2}{I_g N} \tag{50}$$

is the total energy of the target relative to integrated energy of the background in a single azimuth bin of the patch. The point target must be smeared over K_{ta} resolution in azimuth for the target-to-background energy ratio to be unity. Unfortunately this expression for the sharpness ratio, which depends on the target-to-background ratio, strength, the background correlation $|\mu_g|$, the number of range bins N, and the length of the smear M_a and the length of the patch M is too complicated to interpret easily. We do see, though, that as K_{ta} becomes larger, f_4 approaches M_a, and then to detect the moving target with threshold $f_{4t} = 2$, we need a smear length of $M_a = 2$ unweighted resolution elements. We also see that as K_{ta} becomes small, f_4 approaches unity, and we could not detect the moving target. As an example, Fig. 6 shows plots of three examples of f_4 versus M_a, with $K_{ta} = 100$, 10, and 3, for $N = 16$, $M = M_a$, and $|\mu_g| = 0.3$. We see the effect that if the smear length M_a is too small, then there is insufficient phase error (smearing) to detect, and if M_a is too large, then the target-to-background ratio becomes too small to detect the phase error. For comparison, for a conservative indication of a moving target we need $f_{4t} = 2$ to achieve a low false-alarm rate, which we determined by running the algorithm on a large number of images with different backgrounds. Fig. 6 shows that for $K_{ta} = 100$ (i.e., the target/background energy ratio would be unity if the target were smeared over 100 unweighted resolution elements), then f_4 would exceed $f_{4t} = 2$ for a very wide range of M_a (and hence for a wide range of target velocities), whereas for $K_{ta} = 5$, f_4 would exceed $f_{4t} = 2$ only for a limited range of velocities.

The minimum and maximum detectable azimuth velocities and range accelerations are both governed by the minimum and maximum detectable smears, which we define as the values of M_a resulting in $f_{4t} = 2$.

First suppose that we hold the patch length M fixed, and that $M_a < M$. We can solve the equation above for M_a in terms of f_4, yielding

$$M_a = \frac{K_{ta}\beta \pm \sqrt{K_{ta}^2\beta^2 - 8f_{4t}(f_{4t}-1)K_{ta}^3M^2N|\mu_g|}}{4(f_{4t}-1)M^2|\mu_g|} \tag{51}$$

where

$$\beta = K_{ta}^2N - M(f_{4t}-1)(2 + K_{ta}N|\mu_g|). \tag{52}$$

The minimum and maximum detectable smear lengths are given by the positive and negative signs, respectively, in the expression above. There are real solutions only if the term within the square root is nonnegative, which occurs only if

$$K_{ta}^2N \geq M(f_{4t}-1)(2 + K_{ta}N|\mu_g|) + \sqrt{8f_{4t}(f_{4t}-1)K_{ta}M^2N|\mu_g|}. \tag{53}$$

Fig. 7 shows, as an example, the minimum M_a plotted as a function of K_{ta} for $f_{4t} = 2.0$, $|\mu_g| = 0.1$, $N = 16$, and for $M = 64$ and $M = 8$. For larger target-to-background ratios K_{ta}, both curves approach the minimum M_a of $f_{4t} = 2$. As expected, the pair of curves show that, for the smaller values of K_{ta}, the minimum detectable smear is smaller if we use a smaller patch size (keeping $M \geq M_a$). The minimum detectable M_a is minimized for $M = M_a$. We also found that, for typical sets of parameters, the maximum detectable M_a, as a function of M, was greater than M. We limit M_a to be no greater than M to avoid problems with determining the effect of truncating the image of the moving target; hence for determining the maximum detectable M_a we also set $M = M_a$ in which case we have

$$f_4 = \frac{\dfrac{K_{ta}^2M_aN(K_{ta} + M_a|\mu_g|)}{(K_{ta} + M_a^2|\mu_g|)} + 2M_a^2}{K_{ta}^2N + 2M_a^2}. \tag{54}$$

Solving for M_a involves a quartic equation, which can be solved by standard techniques. The complicated solution will be omitted here for the sake of brevity. In the limit of a very bright point target, f_4 approaches M_a, as we saw earlier.

Returning to the case of fixed $M > M_a$, for the case of perfectly uniform clutter, with $|\mu_g| = 0$, the

expression for f_4 simplifies to

$$f_4 = \frac{K_{ta}^2 M_a N + 2M_a M}{K_{ta}^2 N + 2M_a M}. \tag{55}$$

For this case we can solve for the smear length M_a that yields the threshold f_{4t} as

$$M_{a\min} = \frac{f_{4t} K_{ta}^2 N}{K_{ta}^2 N - 2(f_{4t} - 1)M} \tag{56}$$

which approaches f_{4t} for large K_{ta}. This smear length corresponds to the minimum that results in sharpness ratio of f_{4t}. If we take $f_{4t} = 2$ to be required to detect a target, then $M_{a\min} = 2K_{ta}^2 N/(K_{ta}^2 N - 2M)$.

On the other hand, if we use the optimal patch size $M = M_a$, we have

$$f_4 = \frac{K_{ta}^2 M_a N + 2M_a^2}{K_{ta}^2 N + 2M_a^2}. \tag{57}$$

Solving this expression for M_a, we have the minimum and maximum detectable smear lengths to achieve an sharpness ratio of f_{4t} for the case of a perfectly uniform clutter background as

$$M_a = \frac{K_{ta}^2 N \pm \sqrt{K_{ta}^4 N^2 - 8(f_{4t} - 1) f_{4t} K_{ta}^2 N}}{4(f_{4t} - 1)}. \tag{58}$$

For the case of a bright target, the first term within the square root is considerably larger than the second; performing a three-term Taylor-series expansion, we find that

$$M_{a\max} \approx \frac{K_{ta}^2 N}{2(f_{4t} - 1)} - f_{4t} \tag{59}$$

and

$$M_{a\min} \approx f_{4t} + \frac{2(f_{4t} - 1) f_{4t}^2}{K_{ta}^2 N} = 2 + \frac{8}{K_{ta}^2 N} \tag{60}$$

for uniform clutter background and for $f_{4t} = 2$. This shows that the minimum detectable azimuth smear remains near the ideal of $M_{a\min} \approx f_{4t}$ (which has an appropriate value of 2) as long as the target-to-background energy is large.

b) *Sharpness ratio—single-point background*: When the background in the patch consists of a single point target (like a corner reflector), then the background has the form

$$f_g(x, y) = c\delta(x, y). \tag{61}$$

After correction it is smeared over an interval of length approximately $[1 + \alpha(M_a - 1)]$, and its contribution to the sharpness is

$$\mathbf{S}_{1g} = \left(\frac{|c|^2}{[1 + \alpha(M_a - 1)]} \right)^2 \times [1 + \alpha(M_a - 1)] = \frac{|c|^4}{1 + \alpha(M_a - 1)}. \tag{62}$$

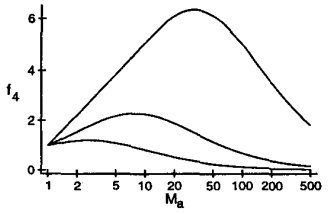

Fig. 8. Predicted sharpness ratio as function of smear length for point-object background. For target/background ratio of 10 (upper curve), 4 (middle curve), and 2 (lower curve).

Then the total sharpness is

$$\mathbf{S}_1 = \mathbf{S}_{1t} + \mathbf{S}_{1g} = \frac{|b|^4}{[M_a + \alpha(1 - M_a)]} + \frac{|c|^4}{[1 + \alpha(M_a - 1)]} \tag{63}$$

and so the sharpness ratio is

$$f_4 = \frac{\mathbf{S}_1(\alpha)}{\mathbf{S}_1(\alpha = 0)} = \frac{\dfrac{|b|^4}{[M_a + \alpha(1 - M_a)]} + \dfrac{|c|^4}{[1 + \alpha(M_a - 1)]}}{|b|^4/M_a + |c|^4}. \tag{64}$$

Now the fraction of the focusing is

$$\alpha \approx k_t = |b|^2/(|b|^2 + |c|^2). \tag{65}$$

Inserting this into the equation above yields

$$f_4 = \frac{\dfrac{|b|^4}{[M_a + (1 - M_a)|b|^2/(|b|^2 + |c|^2)]} + \dfrac{|c|^4}{[1 + (M_a - 1)|b|^2/(|b|^2 + |c|^2)]}}{|b|^4/M_a + |c|^4} = \frac{\dfrac{|b|^4/|c|^4}{M_a + |b|^2/|c|^2} + \dfrac{1}{1 + M_a|b|^2/|c|^2}}{(|b|^4/|c|^4)/M_a + 1} \left(1 + \frac{|b|^2}{|c|^2}\right). \tag{66}$$

Fig. 8 shows f_4 for this case as a function of M_a for three cases (top to bottom): $|b|^2/|c|^2 = 10$, 4, and 2. For this more difficult circumstance, the moving target must contain about four times the energy of the point-like background to be detected over some range of M_a using the sharpness ratio.

Solving the expression for f_{4t} in terms of M_a we arrive at a cubic equation, which we solved by standard techniques. For the sake of brevity, the lengthy solution is omitted here. Of the three roots of the cubic equation, one corresponds to the minimum M_a, a second to the maximum, and the third to a nonphysical value.

B. Performance Prediction by Computer Simulation

We simulated complex SAR images of resolved military targets, simulated the smearing effects typical of target motion, embedded the smeared

images into real SAR images with backgrounds of various types, and tested the detection algorithm to determine performance. The simulated phase errors were quadratic, which are appropriate to either a constant component of azimuth velocity or a constant acceleration component in range. The backgrounds included trees, grass, desert, a subdivision, a highway area, and a motor pool. We simulated target/background ratios of 0.5, 2.0, and 10, and a variety of quadratic phase errors.

We found that the sharpness ratio (f_4) allowed us to distinguish all the cases of target-plus-background from the cases of target absent (i.e., background only) when the target/background energy ratio was 2.0 or 10. There was some overlap of the distributions, however, when the target/background ratio was 0.5.

Some additional conclusions from experiments with simulated moving targets in real backgrounds are as follows. The sharpness ratio f_4 and the degree of image correlation both give much better indications of moving targets than several other features that we investigated, including the rms phase error. However, since the sharpness ratio is several times faster to compute than the degree of image correlation, we strongly prefer to use the sharpness ratio. We also investigated the combination of more than one feature using a likelihood ratio test. This did improve detection performance, but at the expense of sometimes considerable additional computations, and it required having a good estimate of the statistics of the joint probability functions, which we do not yet know for real data. However, once sufficient images of real moving targets are measured, then combining multiple features using the likelihood ratio test should be revisited.

C. Performance Obtained on Real Data

Because we had available only a few images of ground-truthed moving targets, we do not have statistically significant results of detection performance for real moving targets. Nevertheless, what results we have gotten with real data have been excellent. An example is shown in Section IIC.

For the real data we have found that a sharpness ratio of around 2.0 or higher provides a good indication of a moving target with few false alarms.

Our analysis in the previous section does not include the case of the patch size M being smaller than the smear length M_a. We however found that, when the target/back-ground ratio is large, the algorithm can successfully detect the moving targets even when $M_a = 10M$.

If the smearing due to target motion is highly spatially variant (different for different parts of the target), then a simple phase-error-correction algorithm cannot focus all of it at once, and the sharpness may not increase sufficiently to result in a detection.

We investigated potential sources of false alarms.

In one test on a vibrating (but otherwise stationary) target, it was not indicated as a moving target even though the paired-echo sidelobes were purposely kept within the same patch.

Moderately wind-blown trees, the images of which were smeared by several resolution elements, were not indicated as moving targets. This might result from the fact that each branch is moving with different velocity and direction; hence the phase error for each is different, and the net phase error for the image patch as a whole is near zero (and the tree cannot be focused). In general, the algorithm is likely to sense the motion of a single rigid body within an image patch, but not multiple bodies with different motions within the same patch.

We found that a significant source of false alarms is moving glints along the sides of gently curving roads or railways. The point of reflection directly back to the SAR from a gently curving dihedral (like a curb on a road or a guard-rail interacting with the ground) is that point at which the dihedral is perpendicular to the instantaneous line-of-sight. Hence as the SAR platform moves forward, that point on the curve moves forward or backward, depending on whether the curve is convex or concave from the point of view of the SAR. Analysis of the signal history of a moving glint shows it to be indistinguishable from that of a moving point scatterer. So translating glints act very much like moving targets. In addition, they are fairly common. To overcome this false alarm, one can merely be suspicious of any moving target cue that is on a part of a road or rail that is precisely perpendicular to the range direction.

Another potential source of false alarms is any image feature that appears as a very bright, thin line in a single range bin. This could cause a false alarm because 1) the shear averaging algorithm, which weights the phase-difference estimate by the energy of the return in each range bin, would be dominated by the single bright range bin, 2) the phase-error estimate would then just be the phase of the signal history due to that range bin, 3) after focusing all the range bins, that bright range bin would focus to approximately a single bright point while the other range bins would be blurred out, and 4) the bright range bin would dominate the image sharpness calculation, and so the sharpening of that range bin would more than make up for the blurring of the other (dim) range bins. We have seen what appears to be this effect in one image, but further analysis is required to determine whether it was a true false alarm of this type. It might be possible to circumvent this problem by prenormalizing all the range bins before performing shear averaging. One would have the same problem with any higher-order phase-error correction algorithm.

V. CONCLUSIONS

In this paper we have shown that we can detect the presence of moving targets by dividing a complex-valued SAR image into patches, focusing each patch separately, and measuring the sharpness increase in the focused patch. This detection algorithm is sensitive to azimuthal velocities and radial accelerations of the moving target, as these motions induce image smearing that can be focused to improve image sharpness. This is complementary to conventional moving-target indicator radars and dual-phase-center-aperture SARs which sense radial velocities. However, our algorithm can be used with a conventional single-antenna SAR. The algorithm can detect slow azimuth velocities and exquisitely small amounts of radial acceleration, making it effective for targets traveling in any direction. The algorithm can detect any motion that causes a smearing of about two (or more) resolution elements. This assumes that the background is focused so as to be smeared by no more than a resolution element; this is usually achieved with standard autofocus algorithms. The target/background ratio within the patch need be only on the order of unity. The algorithm is fast, requiring fewer computations than needed to form the image. Another useful, but less effective, feature indicative of a moving target is the magnitude of the phase-error estimate.

Since use of the phase error, without requiring an improvement in image sharpness, is the basis for other approaches [9, 10], this approach is expected to have superior detection performance. Its subdivision of the entire image into patches, which increases the integrated target-to-background ratio for patches countaining moving targets, also improves performance over an approach based on the contents of an entire range bin [10].

ACKNOWLEDGMENTS

The moving-target detection algorithm was implemented in different software versions and tested by Chris Bobrowski, Nancy L. Kay, Ann M. Kowalczyk, and Linda E. Elenbogen. We thank John Henry, MIT Lincoln Laboratory, for providing ADTS data on the moving schoolbus.

REFERENCES

[1] Staudaher, F. M. (1990)
Airborne MTI.
In M. I. Skolnik (Ed.), *Radar Handbook* (2nd ed.).
New York: McGraw-Hill, 1990, ch. 16.

[2] Shnitkin, H. (1994)
Joint stars phased array radar antennas.
IEEE AES System Magazine (Oct. 1994), 34–41.

[3] Walker, J. L. (1980)
Range-Doppler imaging of rotating objects.
IEEE Transactions on Aerospace and Electronic Systems, **AES-16** (1980), 23–52.

[4] Ausherman, D. A., Kozma, A., Walker, J. L., Jones, H. M., and Poggio, E. C. (1984)
Developments in radar imaging.
IEEE Transactions on Aerospace and Electronic Systems, **AES-20** (1984), 363–400.

[5] Fienup, J. R. (1989)
Phase error correction by shear averaging.
In *Signal Recovery and Synthesis III*, digest of papers.
Optical Society of America, 1989, 134–137.

[6] Werness, S. A., Carrara, W. G., Joyce, L., and Franczak, D. (1990)
Moving target imaging algorithm for SAR data.
IEEE Transactions on Aerospace and Electronic Systems, **26** (1990), 57–67.

[7] Eichel, P. H., Ghiglia, D. C., and Jakowatz, C. V., Jr. (1989)
Speckle processing method for synthetic-aperture-radar phase correction.
Optics Letters, **14** (1989), 1–3.

[8] Carrara, W. G., Goodman, R. S., and Majewski, R. M. (1995)
Spotlight Synthetic Aperture Radar Signal Processing Algorithms.
Boston: Artech House, 1995.

[9] Moreira, J. R., and Keydel, W. (1995)
A new MIT-SAR approach using the reflectivity displacement method.
IEEE Transactions on Geoscience and Remote Sensing, **33** (1995), 1238–1244.

[10] Barbarossa, S., and Scaglione, A. (1998)
Autofocusing of SAR images based on the product of high-order ambiguity function.
IEE Proceedings, Radar Sonar Navigation, **145** (1998), 269–273.

[11] Muller, R. A., and Buffington, A. (1974)
Real-time correction of atmospherically degraded telescope images through image sharpening.
Journal of the Optical Society of America, **64** (1974), 1200–1210.

[12] Paxman, R. G., and Marron, J. C. (1988)
Aberration correction of speckled imagery with an image-sharpness criterion.
In *Statistical Optics*, Proceedings of SPIE, 976-05, San Diego, CA, Aug. 1988.

[13] Berizzi, F., and Corsini, G. (1996)
Autofocusing of inverse synthetic aperture radar images using contrast optimization.
IEEE Transactions on Aerospace and Electronic Systems, **32** (1996), 1185–1191.

[14] Fienup, J. R. (2000)
SAR autofocus by maximizing sharpness.
Optics Letters, **25** (2000), 221–223.

[15] Henry, J. C. (1991)
The Lincoln Laboratory 35 GHz airborne polarimetric SAR imaging radar system.
Presented at IEEE Aerospace and Electronics Systems Society, 1991 National Telesystems, Atlanta, GA, Mar. 26, 1991.

[16] Morrison, D. P., Eckert, A. C., and Shields, F. J. (1994)
Studies of advanced detection technology sensor (ADTS) data.
In D. A. Giglio (Ed.), *Algorithms for Synthetic Aperture Radar Imagery.*
Proceedings of SPIE, **2230** (1994), 370–378.

[17] Fienup, J. R., and Kowalczyk, A. M. (1995)
Detecting moving targets in SAR imagery by using a phase-error correction algorithm.
Proceedings of SPIE, **2487-30**, Algorithms for Synthetic Aperture Radar Imagery II, Orlando, FL, Apr. 17–21, 1995.

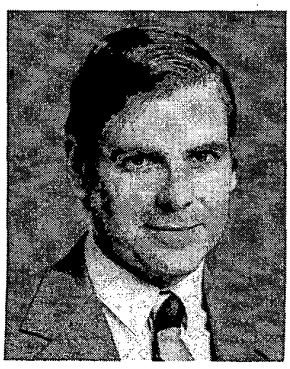

James R. Fienup (M'85—SM'90) was born in St. Louis, MO. He received B.A. degrees in physics and mathematics (magna cum laude) from Holy Cross College, Worcester, MA, in 1970, and the M.S. and Ph.D. degrees in applied physics from Stanford University, Stanford, CA, in 1972 and 1975, respectively. He was a National Science Foundation Graduate Fellow from 1970 to 1972.

Since 1975 he has been a research scientist at Veridian Systems (formerly ERIM), where he is currently the Senior Scientist in EO/IR Sensing Group. His current research activities include phase retrieval and image reconstruction, autofocus and moving target detection algorithms for synthetic aperture radar (SAR), and imaging with sparse apertures.

Dr. Fienup is the author of over 100 papers and holds three patents. He is a fellow of the Optical Society of America, and a fellow of the International Society for Optical Engineering (SPIE). He is the recipient of the SPIE 1979 Rudolph Kingslake Medal and Prize, the International Commission for Optics 1983 International Prize in Optics, and the Best Paper Award for 1990 by the IRIS Specialty Group on Active Imaging. He has chaired the OSA Image Processing Technical Group. He has served as Associate Editor of *Optics Letters*, Topical Editor and Division Editor for *Applied Optics—Information Processing*, and is currently the Editor of the *Journal of the Optical Society of America A*.